Soft parametric resonance for hot carriers in graphene

Samwel Sekwao[1] and Jean-Pierre Leburton[1,2,*]

[1]*Department of Physics and Beckman Institute, University of Illinois, Urbana-Champaign, Urbana, Illinois 61801, USA*

[2]*Department of Electrical and Computer Engineering, University of Illinois, Urbana-Champaign, Urbana, Illinois 61801, USA*

(Received 15 June 2012; published 19 April 2013)

We show that hot carriers scattered by optic phonons in graphene undergo an anomalous parametric resonance when modulated by an ac field, at about half of the frequency $\omega_F = 2\pi eFv_f/\hbar\omega_{\rm op}$, corresponding to ballistic acceleration up to the phonon energy $\omega_F = 2\pi eFv_f/\hbar\omega_{\rm op}$ in the presence of a dc field F. The resonance occurs in the terahertz range and is tunable with dc electric fields. Dephasing between the current and the ac field also exhibits a nonzero minimum at resonance for weak elastic scattering, while increasing monotonously with ac frequency for strong elastic scattering. The overall effect would also manifest in a long-range spatially varying periodic potential.

DOI: 10.1103/PhysRevB.87.155424 PACS number(s): 72.80.Vp

I. INTRODUCTION

The peculiar band structure of graphene with a zero-gap, linear-dispersion relation between energy and momentum, $E = \hbar v_f|k|$ where $v_f \sim 10^8$ cm/s,[1,2] is much larger than the saturation velocity in semiconductors,[3] makes a unique material for studying massless Dirac fermions in solids, with technological opportunities for high-performance electronics. Hence, in high electric fields F, it is well known that carriers can accelerate ballistically before being scattered by high-energy optical phonons (OPs) ($\hbar\omega_{\rm op} \sim 0.2$ eV) causing carrier velocity saturation.[4,5] This produces a back-and-forth motion of carriers in k space between monochromatic OP energy and the Dirac point with a time period $\tau_F = \hbar\omega_{\rm op}/eFv_f$,[6,7] which results in a carrier velocity overshoot[8] and even damped oscillations during the transient to steady state, when the field is suddenly turned on.[6,7] While these oscillations were predicted to occur in GaAs at low temperature so that $\hbar\omega_{\rm op} \gg k_BT$ [$\hbar\omega_{\rm op}$(GaAs) = 36 meV], they were limited to low fields ($F \sim$ 50–100 V/cm, $\tau_F \sim 30$ ps)[6] to prevent intervalley scattering, whereas strong Coulomb scattering arising from the charged dopants would offset the effect. In graphene, the absence of an energy gap guarantees carriers without requiring dopants, while the large OP energy and weak acoustical-phonon (AP) scattering[9] allows its manifestation at room temperature with ramifications in THz technology, since the oscillation frequency $\omega_F = 2\pi/\tau_F \propto F \sim 1$ THz ($F =$ 2 kV/cm) is tunable with the electric field. If a periodic (ac) field is superposed onto the dc field, the frequency of the back-and-forth carrier motion is modulated by the ac frequency, as a parametric oscillator. As a result, the amplitude of the carrier velocity or current oscillations is expected to be resonantly enhanced when the ac frequency ω matches a particular value η of the natural frequency ω_F, i.e., $\omega = \eta\omega_F$.[10] However, there are distinct differences between the usual parametric resonance (PR) and this type of hot-carrier resonance: First, the natural oscillations are strongly damped as a result of the probabilistic nature of the carrier-OP interaction that relaxes carrier energy at different times and momenta once they reach, and even overshoot, the OP energy. Second, the system is strongly dissipative as the OP relaxation is responsible for bringing back the carriers to the low-energy Dirac point. Consequently, the resonance is anticipated to be "soft" i.e., with a broad peak in the oscillation amplitude vs ω, and to manifest for different η values than normal PR.

Because of these distinctive features, we show in this work the anomalous nature of this type of resonance that manifests for $\eta \sim 1/2$ instead of $\eta \sim 2$ in normal PR.[10] We also find that the dephasing between the current and ac field exhibits a minimum as a function of the ac field frequency for weak damping by AP or other low-energy scattering, and softens to become monotonic at high damping for all ac field strengths.

II. OPTIC-PHONON SCATTERING AND HOT-CARRIER MODEL

Our system consists of electrons in the conduction band of graphene under the influence of a spatially homogeneous and time-dependent electric field $F(t)$. The electric field takes the form $F(t) = F_o + F_1\cos(\omega t)$ and is applied along the positive k_x direction, where F_o is a permanent constant field, F_1 is a constant such that $0 < F_1/F_o < 1$, and ω is the frequency of the applied field. The momentum space is divided into the low (I) and high (II) energy regions bounded by the critical momentum k_c that corresponds to electron energy $\hbar v_F k_c = \hbar\omega_{\rm op}$ (Fig. 1). In the low-energy region I, charge carriers are ballistically accelerated towards the critical circle k_c while interacting with low-energy scattering agents (e.g., APs or impurities). In the high-energy region II, the carriers lose all their energy by OP emission and are scattered back into the low-energy region. For this process to occur, the electric-field maximum is low enough such that electrons move back and forth between regions I and II only, with negligible probability to reach $E \geqslant 2\hbar\omega_{\rm op}$.

Because of the probabilistic nature of carrier transport, we solve a large-signal Boltzmann transport equation (BTE) that accounts for low-energy scattering (damping), e.g., by impurities and AP.[7,11] The BTE in the two regions can be written as[7]

$$\frac{\partial f_I(\vec{k},t)}{\partial t} + \frac{eF(t)}{\hbar}\frac{\partial f_I(\vec{k},t)}{\partial k_x} = -\frac{f_I(\vec{k},t) - f_o(\vec{k})}{\tau_{\rm LE}} + \sum_{\vec{k}'} S_{\rm op}(\vec{k}',\vec{k})\, f_{II}(\vec{k}',t), \quad \text{(1a)}$$

$$\frac{\partial f_{II}(\vec{k},t)}{\partial t} + \frac{eF(t)}{\hbar}\frac{\partial f_{II}(\vec{k},t)}{\partial k_x} = -f_{II}(\vec{k},t)\sum_{\vec{k}'} S_{\rm op}(\vec{k},\vec{k}'), \quad \text{(1b)}$$

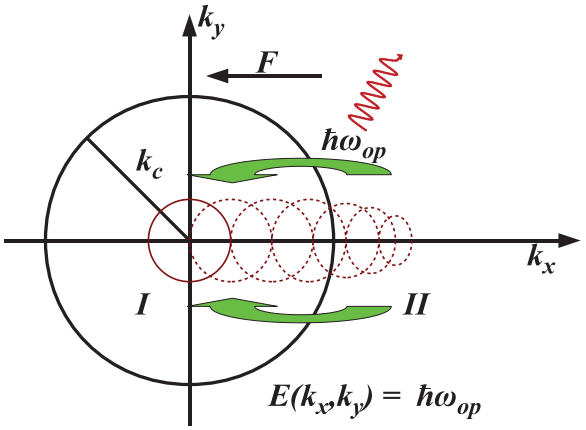

FIG. 1. (Color online) Quasiballistic carrier acceleration followed by OP scattering in the 2D k space of graphene. The circle corresponds to the electronic energy $\hbar\omega_{\rm op}$.

where $f_I(\vec{k},t)$ and $f_{II}(\vec{k},t)$ are the time-dependent momentum distribution functions (DF) in the low- and high-energy regions, respectively, and e is the electronic charge. Equation (1a) describes electron transport at low energy, where the left-hand side (LHS) accounts for the transient drift, while the first term on the right-hand side (RHS) accounts for low-energy scattering, i.e., AP and impurities scattering. The second term on the RHS of Eq. (1a) accounts for low energy carrier repopulation caused OP emission. Equation (1b) describes electron transport at high energy ($E \geqslant \hbar\omega_{\rm op}$), where the LHS and the RHS account for transient drift, and electron depopulation due to OP emission, respectively.[7] In Eq. (1a), the function $f_o(\vec{k})$ is the Fermi-Dirac DF ($k_F > 0$), $S_{\rm op}(\vec{k},\vec{k}')$ is the OP transition rate between the states $\vec{k}$ and $\vec{k}'$, and $\tau_{\rm LE}$ is the relaxation time.[7] In this analysis, the temperature of the graphene sample is assumed to be $T = 300$ K, so $n_q \ll 1$, and we can neglect phonon absorption. However, we observed that our model is also valid at lower T, as the DF profile larger than the thermal broadening is essentially determined by high-field carrier dynamics, as long as the Coulomb scattering (dopant concentration) can be kept weak, as shown in Ref. 7 and later on in this analysis. We note that at this temperature, and if we choose $E_F = k_B T$ above the Dirac point in $f_o(\vec{k})$, the carrier concentration is $n_c \approx 1.8 \times 10^{11}$ cm^{-2}, which is low enough to neglect intercarrier scattering on the DF. Moreover, the hole concentration is even smaller to significantly affect the carrier dynamics in the conduction band so that interband transition can be neglected.[12]

A. Self-consistent solution of Boltzmann transport equation

The procedure is to solve Eq. (1b) for $f_{II}(\vec{k},t)$ and substitute the solution in Eq. (1a) to solve for $f_I(\vec{k},t)$.[7,13] The DFs in the two regions are then matched on the boundary $k = k_c$.

By using the substitution $\kappa = k_x + \beta(t)$, where

$$\beta(t) = -\frac{e}{\hbar}\int_0^t F(s)ds, \tag{2}$$

the LHS of Eq. (1) transforms into $eF[\beta^{-1}(\kappa - k_x)]\partial g_{I,II}/\hbar\partial k_x$, where $g_{I,II}(k_x,k_y;\kappa) = f_{I,II}[k_x,k_y,\beta^{-1}(\kappa - k_x)]$, and β^{-1} is the inverse function of β so that $\beta^{-1}\beta(t) = t$. Consequently, the general solution of Eq. (1b) takes the form

$$f_{II}(k_x,k_y,t) = f_b\{k_y,\beta^{-1}[\beta(t) + k_x - k_x^0]\}M(k_x,k_y,t), \tag{3}$$

where $f_b(k_y,t) = f_{II}(k_x^0,k_y,t)$ is the time-dependent DF evaluated at the boundary $k = k_c$, and $k_x^0 = \sqrt{(k_c)^2 - (k_y)^2}$. The $M(k_x,k_y,t)$ factor given by

$$M(k_x,k_y,t) = \exp\left(-\frac{\hbar}{e}\int_{k_x^0}^{k_x}\frac{dp\,\tau_{\rm op}^{-1}(p,k_y)}{F\{\beta^{-1}[\beta(t) + k_x - p]\}}\right)$$

is the decay function caused by OP emission of hot carriers, and $1/\tau_{\rm op}(\vec{k}) = \sum_{\vec{k}'} S_{\rm op}(\vec{k},\vec{k}')$. Equation (3) is then substituted into Eq. (1a) to solve for $f_I(\vec{k},t)$. The matching conditions $f_b(k_y,t) = f_I(k_x^0,k_y,t) = f_{II}(k_x^0,k_y,t)$ of the two solutions f_I and $f_I I$ at the boundary lead to an integral equation of the form

$$\begin{aligned} f_b(k_y,t) = {} & f_b^1(k_y,t) + \frac{\hbar}{(2\pi)^2 e}\int_{-k_x^0}^{k_x^0} dp \\ & \times \int d\vec{k}'\, S_{\rm op}(\vec{k}',\vec{k})\Big|_{k_x=p} f_{II}(\vec{k}',t') \\ & \times \exp\left(\frac{t'-t}{\tau_{\rm LE}}\right)\Big/ F(t'), \end{aligned} \tag{4}$$

where the function $f_b^1(k_y,t)$ is the solution $f_I(k_x^0,k_y,t)$ in the absence of OP scattering, and t' is a retarded time such that $\beta(t') = \beta(t) + k_x^0 - p$ (see Supplemental Material in Ref. 14). The second term on the RHS of Eq. (4) accounts for the contribution of OP emission to the DF at the boundary, and the summation is taken over states $\vec{k}'$ in the high-energy region. Equation (4) is solved by iteration, and the solution for $f_b(k_y,t)$ is expressed as a series,

$$f_b(k_y,t) = f_b^1(k_y,t) + f_b^2(k_y,t) + f_b^3(k_y,t) + \cdots \tag{5}$$

which converges since the function $M(k_x,k_y,t)$ is a decreasing exponential and $f_b^n \propto (1/2\pi)^{n-1}$. The solution for $f_b(k_y,t)$ used throughout this analysis is obtained by neglecting terms of $O[(1/2\pi)^3]$ and higher in the series (5). Once $f_b(k_y,t)$ is known, the DFs in both regions are readily obtained.

The two-dimensional (2D) current density on the plane is given by

$$J_x(t) = -4ev_F\sum_{\vec{k}} f(\vec{k},t)\cos(\phi), \tag{6}$$

where ϕ is the angle between $\vec{k}$ and the k_x axis, and $f(\vec{k},t)$ is the DF in the two regions.

III. RESULTS

In this analysis, we use $F_o = 1$ kV/cm and express the applied frequency in units of ω/ω_F. We also define a dimensionless damping parameter γ to gauge the strength of low-energy scattering as $\gamma = \tau_{\rm op}(k = 1.5k_c)/\tau_{\rm LE}$.[7] We choose $\tau_{\rm op}$ for $k = 1.5k_c$ as the intermediate value between k_c and $2k_c$ as $1/\tau_{\rm op}(k_c) = 0$.

Figure 2 shows the current density versus time for different values of γ and two field strengths at resonance, i.e., when

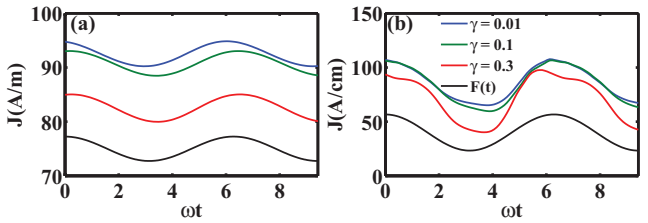

FIG. 2. (Color online) Current density for three different values of the damping γ at resonance ($\omega \approx 0.56\omega_F$). (a) $F_1/F_o = 0.1$; (b) $F_1/F_o = 0.8$.

$\omega \approx 0.56\omega_F$ (see Fig. 3). It is seen that the amplitudes of current density oscillations increase as the applied field F_1 increases compared to F_o as a larger population of electrons escapes low-energy scattering to reach the OP energy. At the same time, electrons also reach lower velocities during the negative cycles of F_1. For this reason, the current density swing increases with F_1/F_o. One also notices distortions in the current density oscillations at large fields [Fig. 2(b)] as the electron population competes between the natural oscillations at ω_F and the oscillations imposed by the F_1 field. As expected, it is also seen that the current density amplitude decreases with increasing γ as a result of increased electron scattering in the low-energy region, thereby lowering the carrier velocity.

Figure 3 shows plots of current density amplitude versus frequency for different values of γ and F_1/F_o. In the figure, the amplitude is defined as the difference between the maximum and minimum values of the current density. As seen from the plots, parametric resonance is achieved when $\omega/\omega_F \approx 0.56$. This unexpected result is due to the fact that electrons take about $\tau_F \sim \hbar k_c/eF$ to reach the OP energy, and an additional τ_F to lose their energy once they reach the OP energy, as they can still accelerate before losing their energy. Consequently, the oscillation period is about $2\tau_F$ and $\omega_{\text{resonance}} \sim \omega_F/2$, which is the same as the current oscillations arising during the transient in the presence of the dc field F_o alone.[7,15] This anomalous value is due to the fact that the modulation of the ac field acts only upon the first half of the natural period, i.e., when carriers are field driven toward the OP energy, while the second half of the period when OPs are emitted is stochastic with a more complicated dependence on the field [see Eq. (3)], which is why the PR frequency is not exactly half of the natural frequency ω_F. From the figure, the oscillation amplitudes

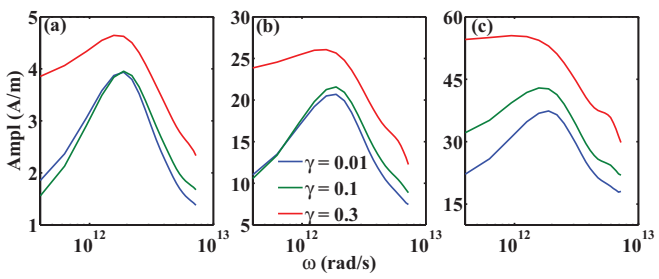

FIG. 3. (Color online) Current density amplitude vs frequency for three different values of the damping parameter γ. (a) $F_1/F_o = 0.1$; (b) $F_1/F_o = 0.5$; (c) $F_1/F_o = 0.8$.

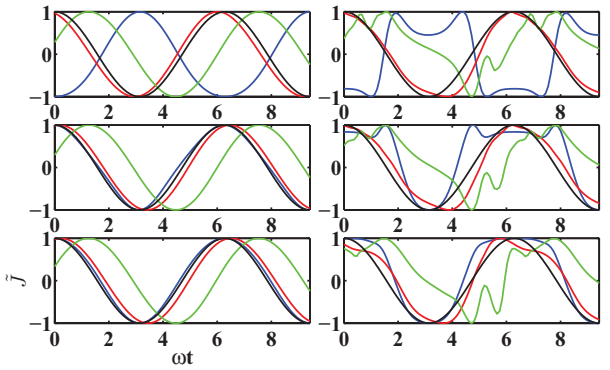

FIG. 4. (Color online) Normalized values of the oscillating part of the current density vs time. Left column, $F_1/F_o = 0.1$; right column, $F_1/F_o = 0.8$. Top row: $\gamma = 0.01$; middle row: $\gamma = 0.1$; and bottom row: $\gamma = 0.3$. Blue curve: $\omega/\omega_F = 0.001$; red curve: $\omega/\omega_F \approx 0.56$; green curve: $\omega/\omega_F = 2.3$; and black curve: normalized ac field.

increase with γ, which as explained in Fig. 2 is due to increased scattering at low energy, sending back electrons close to the $\mathbf{k} = 0$ region, thereby further reducing the minimum values of the current density. The maximum values of the current density are not as affected because a substantial population of electrons is still able to reach high energies, even at high γ. Also, we see from the plots that the amplitude increases with F_1/F_o, as expected, since the difference between current density maxima and minima increases with F_1/F_o. Even though PR is achieved, it is rather "soft" because of the strongly dissipative nature of the back-and-forth motion of charge carriers in the constant field followed by OP emission. Obviously, this effect is more pronounced for the higher values of γ (low-energy scattering) and F_1/F_o (OP scattering) seen in the figure.

Figure 4 shows normalized current densities and electric fields versus time for different values of the parameters ω/ω_F and γ at low electric fields ($F_1/F_o = 0.1$, left column), and high fields ($F_1/F_o = 0.8$, right column). At low fields, the current is sinusoidal as expected from the linear response to the field. It is also observed that at very low frequencies ($\omega/\omega_F = 0.001$) and in the quasiballistic regime ($\gamma = 0.01$, top left column), the current density is 180° out of phase with the field. In this case, as the field slowly decreases from $t = 0$ to $t = \pi/\omega$, the electronic system evolves adiabatically from a regime in high fields to that in low fields, which depletes the charge carriers in the high-energy region ($k > k_c$) and increases their concentration in the low-energy region ($k < k_c$). The current increases as the number of electrons with high k_x values ($k_c/2 < k_x < k_c$) in the low-energy region increases as a result of quasiballistic transport that results in a streamed DF. This situation is clearly seen in Fig. 5 (top row, first two panels), which shows the change in the DF with time $\Delta f = f[\omega t = (n+1)\pi/2] - f[\omega t = n\pi/2]$. From $t = \pi/\omega$ to $t = 2\pi/\omega$, the current decreases as the field increases because the electrons that penetrate deep into the high-energy region ($k > k_c$) with $k_x \gg k_y$ are scattered by OP emission equally to all $k' = k - \omega/v_f$ values. Indeed, the absence of q (phonon wave-vector) dependence in the deformation potential

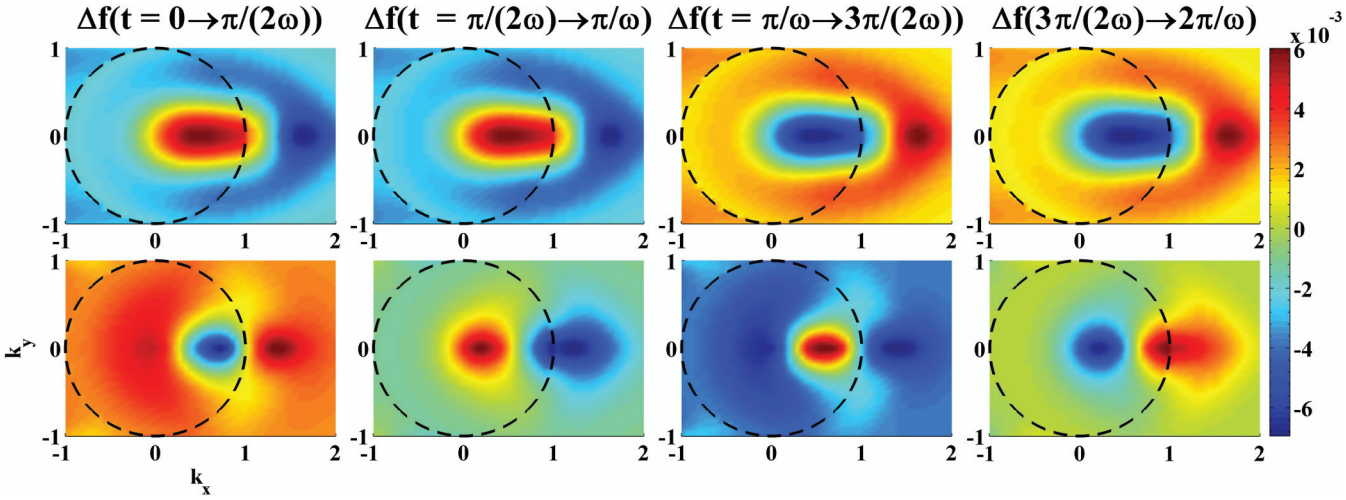

FIG. 5. (Color online) 2D color plot of the electron distribution function difference Δf (as defined in the text, and normalized to the carriers density) in k space (normalized units of k/k_c) at four different times for field ratio $F_1/F_o = 0.1$ and damping $\gamma = 0.01$. Dashed circles correspond to the boundary $k = k_c$ between the low- and high-energy regions. Top row: $\omega/\omega_F = 0.001$. Bottom row: $\omega/\omega_F = 0.56$.

OP matrix element contributes to randomizing the DF,[16] specifically populating low-energy **k** states away from the field direction. This effect results in lowering the current (Fig. 5, top row, last two panels). In Fig. 4 (left column, top), we see that the phase between the current and the field reaches a minimum for frequencies approaching resonance ($\omega/\omega_F = 0.56$). This effect is better understood as the field increases from $t = \pi/\omega$ to $t = 3\pi/2\omega$, then to $t = 2\pi/\omega$, when the ac and the dc fields combine to enhance the back-and-forth motion of carriers between the low-energy **k** states (Fig. 5, bottom row, third panel) and the high-energy **k** states (fourth panel and first panel). For frequencies higher than resonance ($\omega/\omega_F \gg 0.56$), the dephasing between current and electric field starts to increase again (Fig. 6).

One also observes that as low-energy damping increases ($\gamma = 0.1$ and $\gamma = 0.3$; Fig. 4, left column), the dephasing between the current and the field at frequencies below resonance decreases (Fig. 6), as low-energy collisions result in diffusive transport that scatter electrons with high k_x states, thereby changing the streamed DF into a wider (k_y states) DF with lower current density. At intermediate damping ($\gamma = 0.1$), there is even a slight maximum before resonance, but above resonance the dephasing increases monotonically for all damping.

In higher ac fields (Fig. 4, right column), aside from the fact that the current curves are distorted by transport nonlinearity caused by competition between the dc and ac fields, our results concerning the phase difference between the oscillating F_1 field and the current densities are qualitatively the same. One notices, however, that the distortions do not affect the current at resonance, which remains quasisinusoidal. The effect of γ on the current density phase is also seen in Fig. 6. As expected, current density lags behind the electric field before resonance, but the dephasing also drops around resonance for low damping.

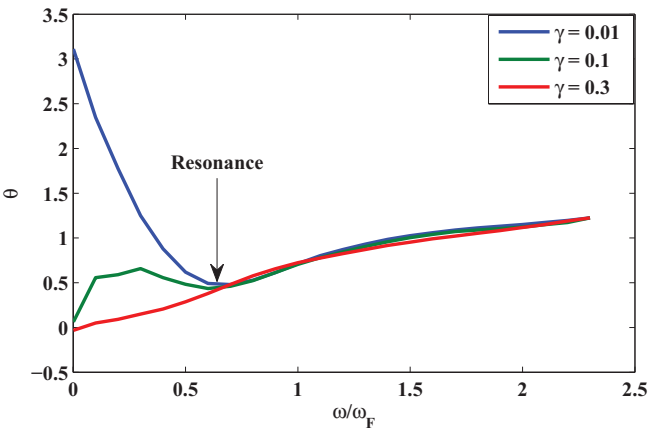

FIG. 6. (Color online) Phase of the current density [compared to $F(t)$] for different values of the damping γ and field ratio $F_1/F_o = 0.1$.

IV. CONCLUSIONS

Although our analysis is performed for time-dependent ac fields in the condition of spatial uniformity, it is also valid in the inverse condition of long-range periodically (oscillatory) modulated potential $V(x) = V(x + d)$ in the steady state. This can be seen from Eqs. (1), where the time-dependent differential $\partial/\partial t$ operator of the BTE LHS is replaced by the spatially varying $v_f \cos\phi\,\partial/\partial x$ operator, for which $\phi \sim 0$ in streamed DFs. Therefore, by making the substitution $t \to x/v_f$ in our formalism, the resonance condition between the periodic potential and the hot-carrier dynamics will arise for $F_o = \hbar\omega_{\rm op}/\eta$ed. in the presence of an external field F_o, which could be used as field detector.

Let us notice that for carrier oscillations to occur in graphene, the electric field has to be high enough to escape low-energy scattering agents, but not too high as to overshoot the OP energy.[7] Also, at high damping, more scattering occurs in the low-energy region and the resulting oscillations are promptly damped. This problem persists even with the addition

of a high-amplitude ac field, and hence the wider resonance peak at high γ in Fig. 3. As a result, clean graphene samples should be used with low values of F_1/F_o for this effect to be observed, and be the basis for novel device applications either as a THz source or detector.

ACKNOWLEDGMENTS

This work was supported by ARO Grant No. W911NF-11-1-0434. The authors gratefully acknowledge the use of the Turing cluster maintained and operated by the Computational Science and Engineering Program at the University of Illinois.

*jleburto@illinois.edu

[1] R. Saito, G. Dresselhaus, and M. S. Dresselhaus, *Physical Properties of Carbon Nanotubes* (Imperial College Press, London, 1998).

[2] M. I. Katsnelson, Mater. Today **10**, 20 (2007).

[3] S. Tiwari, *Compound Semiconductor Device Physics* (Academic, San Diego, CA, 1992).

[4] W. Shockley, Bell Syst. Tech. J. **30**, 990 (1951).

[5] A. C. Ferrari, J. C. Meyer, V. Scardaci, C. Casiraghi, M. Lazzeri, F. Mauri, S. Piscanec, D. Jiang, K. S. Novoselov, S. Roth, and A. K. Geim, Phys. Rev. Lett. **97**, 187401 (2006).

[6] A. Matulionis, J. Pozela, and A. Reklaitis, Phys. Status Solidi A **31**, 83 (1975).

[7] S. Sekwao and J.-P. Leburton, Phys. Rev. B **83**, 075418 (2011).

[8] H. Kroemer, Solid-State Electron. **21**, 61 (1978).

[9] V. Perebeinos, J. Tersoff, and P. Avouris, Phys. Rev. Lett. **94**, 086802 (2005).

[10] F. Arscott, *Periodic Differential Equations* (Pergamon, New York, 1964).

[11] Indeed, if for elastic deformation potential acoustic phonon, relaxation-time approximation is legitimate, for ionized impurity scattering it is also reasonable within a momentum relaxation-time expression. See Ref. 16, p. 115. See also Ref. 22 in A. Barreiro, M. Lazzeri, J. Moser, F. Mauri, and A. Bachtold, Phys. Rev. Lett. **103**, 076601 (2009).

[12] This approximation does not affect the validity of our analysis, as one can always apply it to bilayer graphene where the band gap can be tailored so that $E_G > \hbar\omega_{\rm op}$. See, e.g., T. Ohta, A. Bostwick, T. Seyller, K. Horn, and E. Rosenberg, Science **313**, 951 (2006).

[13] J. Leburton and R. Evrard, J. Low Temp. Phys. **32**, 323 (1978).

[14] See Supplemental Material at http://link.aps.org/supplemental/10.1103/PhysRevB.87.155424 for the complete derivation of Eq. (4).

[15] We note that in GaAs, the current oscillations period matches τ_F, unlike in graphene. However, no PR study has been reported.

[16] K. Hess, *Advanced Theory of Semiconductor Devices* (IEEE, Piscataway, NJ, 2000).